Advances in Materials Research, *Vol.3, No. 1 (2014) 1-21*
DOI: http://dx.doi.org/10.12989/amr.2014.3.1.001

Analysis of a three-dimensional FEM model of a thin piezoelectric actuator embedded in an infinite host structure

Xiaohu Zeng, ZhufengYue*, Bin Zhao and S.F. Wen

School of Mechanics and Civil engineering & Architecture, *Northwestern Polytechnical University*, *Xi'an Shaanxi 710129*, *PR China*

(Received April 8, 2013, Revised December 18, 2013, Accepted January 10, 2013)

Abstract. In this paper, we adopted a two-dimensional analytical electro-elastic model to predict the stress distributions of the piezoelectric actuator in 3D case. The actuator was embedded in an elastic host structure under electrical loadings. The problem is reduced to the solution of singular integral equations of the first kind. The interfacial stresses and the axial normal stress in both plane stress state and plane strain state were obtained to study the actuation effects being transferred from the actuator to the host. The stress distributions of the PZT actuator in different length and different thickness were analyzed to guarantee the generality. The validity of the present model has been demonstrated by application of specific examples and comparisons with the corresponding results obtained from the Finite Element Method.

Keywords: piezoelectric actuator; the 3D FEM model; actuation effect; stress distribution

1. Introduction

Piezoelectric ceramics is a kind of inorganic nonmetallic materials which can realize interconversion between electric energy and mechanical energy. With the emergence of new piezoelectric ceramic materials, the concept of using a network of piezoelectric actuators and sensors to form a self-controlling and self-monitoring smart system in advanced structural design has drawn considerable interests among the research communities. And now the piezoelectric ceramic actuators have been used in the design of different advanced structures, such as large scale space structure, aircraft structures, satellites and bridges.

Piezoelectric ceramic actuators, which are attached to or embedded in a structure, can produce a mechanical deformation under an applied electric field. Then the deformation in turn deform the host structure through load transfer at the interface to generate axial forces, shear forces and bending moments on the structure (Wang *et al*. 2000). For a piezoelectric ceramic actuator in a smart structure system, one of the most fundamental issues is to determine the actuation effects being transferred from the actuator to the host and the local stress distribution around the actuator (Wang *et al*. 2001). In order to obtain the actuation effect and avoid the difficulties associated with the complicated interfaces between the actuators and host structures, some simplified actuator models have been applied to simulate the actuation process of bonded and embedded thin sheet

*Corresponding Author, Ph.D., E-mail: zengxiaohu@mail.nwpu.edu.cn

http://www.techno-press.org/?journal=amr&subpage=7 ISSN: 2234-0912 (Print), 2234-179X (Online)

actuators.

Crawley and de Luis first put forward a beam-like structure with surface bonded and embedded thin sheet piezoelectricactuators to study the stresses transferred by the actuator to the host beam (Crawley *et al*. 1987, Crawley *et al*.1990). In the analysis, the axialstress of the actuator was assumed to be uniform across its thickness and the host structure was treatedas a Bernoulli-Euler beam.Im and Atluri(1989) modified the actuator model to study a beam with surface bonded a piezoelectric actuator under general loading. Lin and Rogers (1993) proposed a refined model based on the plane stress state to study the electromechanical behavior of abeam with symmetrically surface-bonded actuator patches.

Plate and shell models have also been proposed to study the electromechanical behavior of piezoelectric actuator bonded and embedded in a host structure. The classical laminate plate theory was applied tothe design of piezoelectric claminate for bending and torsion modal control by Lee and Moon (1989). Tzou and Gadre (1989) proposed an analytical model of multi-layered thin shells with distributed piezoelectric actuators. The kinematic equations of the model were obtained and verified by experiment. A consistent plate model which is a simple extension from the one-dimensional beam model to the two-dimensional plate model was proposed by Crawley and Lazarus(1991). Other typical examples for simulating piezoelectric actuators include the works in (Wang, B.T. *et al*. 1991, Zhuk *et al*. 2010, Qiu *et al*. 2007, Kumar *et al*. 2008, Zheng *et al*. 2009).

Wang proposed a one-dimensional elasticity equation-based actuator model to study the static load transfer between a thin piezoelectric actuator and an elastic host structures/an anisotropic host structures when the system is subjected to in-plane electrical loadings (Wang *et al*. 2000, Wang *et al*. 2001). The singular stress field around the piezoelectric actuator tips can be obtained from the model. And the actuator model is further modified to study the stress distributions when the piezoelectric actuator is under varying electric loadings, with the effect of both the longitudinal and the transverse deformations of the actuators being considered (Wang *et al*. 2006).

A two-dimensional analytical model of the coupled electromechanical behavior of a thin sheet piezoelectric ceramic actuator embedded in an elastic host structure under in-plane mechanical and electrical loadings was proposed by Zhao and Wang (2012) to study the stresses transferred from the actuator to the host. But the external load applied on the model surface would influence the precision of the test results and the analysis in 3D situation was slightly insufficient.

In this paper, the same analytical model under electrical loadings only was adopted to predict the stress distributions of the piezoelectric actuator in 3D case. This model could avoid the error caused by applying the external load on the model surface. The validity of the two-dimensional model has been demonstrated by application of specific examples and comparisons with the corresponding results obtained from the Finite Element Method.

2.Analysis of a single piezoelectric actuator embedded in a host structure

A piezoelectric actuator made of thin-sheets embedded in a homogeneous and isotropic elastic medium is studied here, as shown in Fig. 1. The length and the width of the actuator are denoted as 2a and h respectively. The poling direction of the actuator is along the y-axis. And a uniform electrical field is applied along the poling direction by applying a voltage between the upper and the lower surfaces of the actuator, simplified in Fig. 1with. In the paper, this model was adopted to predict the stress distributions of the piezoelectric actuator in 3D case. The deformation of the

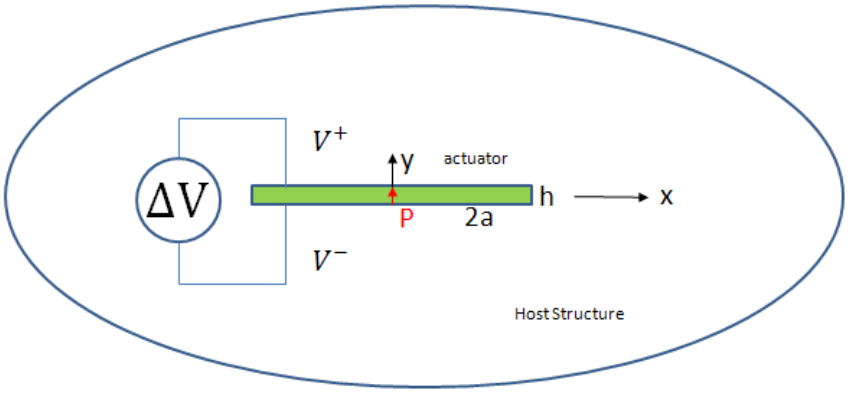

Fig.1 Schematic of an actuator embedded in a host structure

actuator in z-axial direction is very small, so its influence isn't taken into consideration. The validity of the present model can be demonstrated in the following part.

2.1 The actuator model

The actuator studied here can be simulated as a 2D model subjected to the electrical field, the normal stress and the shear stress by simple force analysis, as shown in Fig. 2. The stresses distribution of a small part of the actuator is given in Fig. 2(a). In order to simplify the analysis, the stresses are decomposed in Fig. 2(b). In the next part, the detail description of the relations between Fig. 2(a) and Fig. 2(b) will be discussed. In the figure, the superscript + and the superscript – indicate the components applied on the upper surface and the lower surface of the actuator respectively. The v denotes the displacement in *y*-axial direction, and u denotes the displacement in x-axial direction.

2.2 Formulation of the problem

2.2.1 Equilibrium equations

From Fig. 2 (a) we can get: $$\begin{cases} d\sigma_x \cdot dy + (\tau^+ - \tau^-) \cdot dx = 0 \\ (\sigma^+ - \sigma^-) \cdot dx + (\tau^R - \tau^L) \cdot dy = 0 \end{cases} \tag{2-1}$$

$$\because \ \tau^+ - \tau^- = \frac{\partial \tau}{\partial y} \cdot dy \ , \ \sigma^+ - \sigma^- = \frac{\partial \sigma}{\partial y} \cdot dy \ , \ \tau^R - \tau^L = \frac{\partial \tau_{xy}}{\partial x} \cdot dx \tag{2-2}$$

$$\text{For} \ \ h \to 0 \begin{cases} \dfrac{d\sigma_x}{dx} + \dfrac{\tau^+ - \tau^-}{h} = 0 \Rightarrow \dfrac{d\sigma_x}{dx} + \dfrac{\tau}{h} = 0 \\ \dfrac{\partial \tau_{xy}}{\partial x} + \dfrac{\sigma^+ - \sigma^-}{h} = 0 \Rightarrow \dfrac{\partial \tau_{xy}}{\partial x} + \dfrac{\sigma}{h} = 0 \end{cases} \tag{2-3}$$

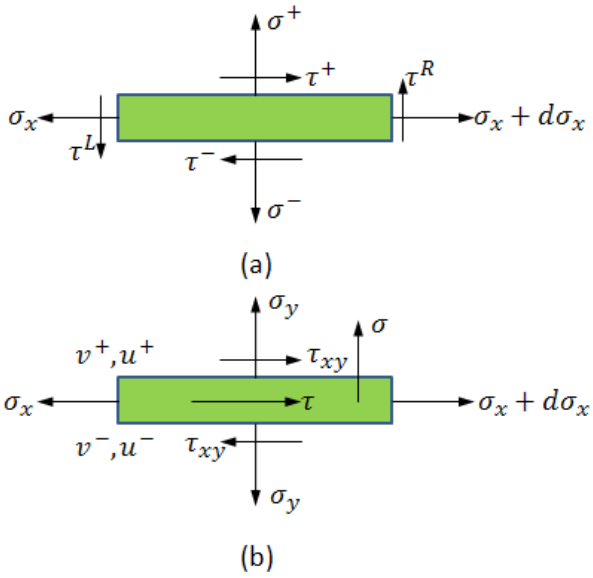

Fig. 2 The actuator model. (a) Original loading status. (b) Changed loading status

$$\therefore \sigma_x = -\int_{-a}^{x} \frac{\tau}{h} \cdot dx \;\; \tau_{xy} = -\int_{-a}^{x} \frac{\sigma}{h} \cdot dx \tag{2-4}$$

$$\text{Where} \begin{cases} \sigma_y = \frac{1}{2}\left(\sigma^+ + \sigma^-\right) & \sigma = \sigma^+ - \sigma^- \\ \tau_{xy} = \frac{1}{2}\left(\tau^+ + \tau^-\right) & \tau = \tau^+ - \tau^- \end{cases} \tag{2-5}$$

2.2.2 Constitutive equations

The following general constitutive equations give the relation between the stress, the strain and the electrical fields of the piezoelectric actuator model.

$$\begin{cases} \sigma_x = C_{11}\varepsilon_x + C_{12}\varepsilon_y - e_1 E_y \\ \sigma_y = C_{21}\varepsilon_x + C_{22}\varepsilon_y - e_2 E_y \\ \tau_{xy} = C_{31}\gamma_{xy} \end{cases} \tag{2-6}$$

where, C_{11}, C_{12}, C_{21}, C_{22}, C_{31} are elastic stiffness parameters, e_1 and e_2 are piezoelectric constants.

2.2.3 Crack Solution

The following dislocation density functions are introduced from the theory of dislocation and crack.

$$\Phi(x)=\frac{d}{d(x)}[u(x,0^{+})-u(x,0^{-})]\ \Psi(x)=\frac{d}{d(x)}[v(x,0^{+})-v(x,0^{-})] \tag{2-7}$$

where $\Phi(x)$ is the dislocation density function in u direction and $\Psi(x)$ is the dislocation density function in v direction.

$$\therefore \begin{cases} \gamma_{xy}=\dfrac{u^{+}-u^{-}}{h}=\dfrac{1}{h}\int_{-a}^{x}\phi dx \\ \varepsilon_{y}=\dfrac{v^{+}-v^{-}}{h}=\dfrac{1}{h}\int_{-a}^{x}\psi dx \end{cases} \tag{2-8}$$

From the continuity condition at y=0, we can get the following equations:

$$\sigma_{y}^{+}=\sigma_{y}^{-}\ \tau_{xy}^{+}=\tau_{xy}^{-} \qquad \text{y=0} \tag{2-9}$$

According to equation (2-9), the general solution for the stress components can be obtained through the following integral equations:

$$\begin{cases} \tau_{xy}(\phi)=\dfrac{2G}{\pi(k+1)}\int_{-a}^{a}\dfrac{\phi(\xi)}{x-\xi}d\xi \\ \sigma_{y}(\psi)=\dfrac{2G}{\pi(k+1)}\int_{-a}^{a}\dfrac{\psi(\xi)}{x-\xi}d\xi \qquad |x|<a \\ \varepsilon_{x}^{(1)}=\varepsilon_{x}^{(1)}(\psi) \end{cases} \tag{2-10}$$

where G is modulus of rigidity, υ is Poisson Ratio and k is Kolosov's constant.

$$k=\begin{cases} 3-4\upsilon & \textit{for plane strain} \\ \dfrac{3-4\upsilon}{1-\upsilon} & \textit{for plane stress} \end{cases} \tag{2-11}$$

2.2.4 Boundary conditions

From Fig. 1, we can see that no boundary conditions are exerted to the actuator model. Then we can get the following equations.

$$\begin{cases}\sigma_y(\psi)=-\sigma_y \\ \tau_{xy}(\phi)=-\tau_{xy}\end{cases} \quad y=0 \quad |x|<a \tag{2-12}$$

$$u(x,0^+)-u(x,0^-)=0\ ,\ v(x,0^+)-v(x,0^-)=0\ ,\ |x|\geq a \tag{2-13}$$

The above equations can be expressed by the following singular integral equations

$$\int_{-a}^{a}\frac{\phi(\xi)}{x-\xi}d\xi=-\frac{\pi(k+1)}{2G}\tau_{xy} \qquad |x|<a \tag{2-14}$$

$$\int_{-a}^{a}\frac{\psi(\xi)}{x-\xi}d\xi=-\frac{\pi(k+1)}{2G}\sigma_y \qquad |x|<a \tag{2-15}$$

And

$$\int_{-a}^{a}\phi(\xi)d\xi=0 \quad \int_{-a}^{a}\psi(\xi)d\xi=0 \tag{2-16}$$

The equations (2-14) and (2-15) can be solved by expanding $\psi(\xi)$ and $\phi(\xi)$ when we use Chebyshev polynomials, as follows

$$\varphi(\xi)=\sum_{j=0}^{\infty}c_jT_j(\frac{\xi}{a})/\sqrt{1-(\frac{\xi}{a})^2}\ \ \psi(\xi)=\sum_{j=0}^{\infty}d_jT_j(\frac{\xi}{a})/\sqrt{1-(\frac{\xi}{a})^2} \tag{2-17}$$

where, T_j are Chebyshev polynomials of the first kind, c_j and d_j are unknown coefficients. According to the orthogonality conditions of the Chebyshev polynomials, $c_0=0$ and $d_0=0$ can be got. Then we can obtain the following equations.

$$\sum_{j=1}^{\infty}c_jU_{j-1}(\frac{x}{a})=\frac{k+1}{2G}\tau_{xy}? \qquad |x|<a \tag{2-18}$$

$$\sum_{j=1}^{\infty}d_jU_{j-1}\left(\frac{x}{a}\right)=\frac{k+1}{2G}\sigma_y \qquad |x|<a \tag{2-19}$$

where U_j is Chebyshev polynomials of the second kind.

If the Chebyshev polynomialsarecut to the Nth term and considering the following collocation points along the actuator,

$$x_k=a\cos(\frac{k\pi}{N}),\quad k=1,2,\cdots N \tag{2-20}$$

Then the equations (2-18) and (2-19) can be simplified to the following linear algebraic equations:

$$\sum_{j=1}^{N} c_j \frac{\sin(j\frac{k\pi}{N})}{\sin(\frac{k\pi}{N})} = \frac{k+1}{2G}\tau_{xy} \qquad j,k = 1,2,\cdots N \tag{2-21}$$

$$\sum_{j=1}^{N} d_j \frac{\sin(j\frac{k\pi}{N})}{\sin(\frac{k\pi}{N})} = \frac{k+1}{2G}\sigma_{y} \qquad j,k = 1,2,\cdots N \tag{2-22}$$

Once the unknown coefficients c_j and d_j are determined, the stress distribution of the crack can be obtained from equations (2-21) and (2-22).

2.2.5 Whole Plane Solution

Because a bonded or embedded actuator is simulated as an electroelastic line, the strain along the y-axial direction should be taken into account. It is determined by the normal stress and shear stress, so we describe it as Eq. (2-23).

$$\varepsilon_x^{(2)} = \varepsilon_x^{(2)}(\tau,\sigma) \tag{2-23}$$

We can see that the strain ε_x in Eq. (2-6) consists of two parts: $\varepsilon_x^{(1)}(\psi)$ and $\varepsilon_x^{(2)}(\tau,\sigma)$

$$\therefore \varepsilon_x = \varepsilon_x^{(1)}(\psi) + \varepsilon_x^{(2)}(\tau,\sigma) \tag{2-24}$$

2.2.6 Summary of the equations

The following equations can be obtained fromequations (2-4), (2-6), (2-8) and (2-10).

2.2.7 Solution of the problem

$$\begin{cases} -\int_{-a}^{x} \frac{\tau}{h}\cdot dx = C_{11}\varepsilon_x + C_{12}\frac{1}{h}\int_{-a}^{x}\psi\cdot dx - e_1 E_y \\ -\sigma_y = C_{21}\varepsilon_x + C_{22}\frac{1}{h}\int_{-a}^{x}\psi dx - e_2 E_y \\ -\tau_{xy} = C_{31}\frac{1}{h}\int_{-a}^{x}\phi dx \\ -\int_{-a}^{x}\frac{\sigma}{h}dx = C_{31}\frac{1}{h}\int_{-a}^{x}\phi dx \\ \tau_{xy} = \frac{2G}{\pi(k+1)}\int_{-a}^{a}\frac{\phi(\xi)}{x-\xi}d\xi \\ \sigma_y = \frac{2G}{\pi(k+1)}\int_{-a}^{a}\frac{\psi(\xi)}{x-\xi}d\xi \\ \varepsilon_x = \varepsilon_x^{(1)}(\psi) + \varepsilon_x^{(2)}(\tau,\sigma) \end{cases} \tag{2-25}$$

From the above seven equations, the solution of the problem can be obtained step by step.

We can get ε_x from equation (2-31)

In order to simplify the analysis, we determine $\varepsilon_x^{(1)}(\psi)$ as $\varepsilon_x^{(1)}(\psi) = -\upsilon\varepsilon_y$. For $\varepsilon_x^{(2)}(\tau,\sigma)$, it can be obtained through the method got from Ref.(X.D. Wang *et al*. 2000), as follows:

$$\varepsilon_x^{(2)}(\tau,\sigma) = \varepsilon_x(x,0)\big|_{host} = \frac{2}{\pi\bar{E}}\int_{-a}^{a}\frac{\tau(\xi)}{x-\xi}d\xi \quad \bar{E} = \frac{8(1-\upsilon)E}{(1+\upsilon)(3-4\upsilon)} \tag{2-32}$$

$$\sigma_x = E_a\varepsilon_x - e_a E_y \tag{2-33}$$

$$\varepsilon_x(x)|_{actuator} = -\frac{1}{E_a h}\int_{-a}^{x}\tau(\xi)d\xi + \frac{e_a}{E_a}E_y \quad |x| < a \text{ (} \tag{2-34}$$

$$\varepsilon_x|_{actuator} = \varepsilon_x|_{host} \quad |x| < a \quad y = 0 \tag{2-35}$$

$$\therefore \frac{2}{\pi\bar{E}}\int_{-a}^{a}\frac{\tau(\xi)}{x-\xi}d\xi = -\frac{1}{E_a h}\int_{-a}^{x}\tau(\xi)d\xi + \frac{e_a}{E_a}E_y \tag{2-36}$$

$$\frac{2}{\pi\bar{E}}\int_{-a}^{a}\frac{\tau(\xi)}{x-\xi}d\xi + \frac{1}{E_a h}\int_{-a}^{x}\tau(\xi)d\xi = \frac{e_a}{E_a}E_y \tag{2-37}$$

$$\int_{-1}^{1}\frac{\bar{\tau}(\zeta)}{\eta-\zeta}d\zeta + \lambda\int_{-1}^{\eta}\bar{\tau}(\zeta)d\zeta = P\text{?} \quad |\eta| < 1 \tag{2-38}$$

where, $\lambda = \dfrac{\pi\bar{E}a}{2E_a h}$ $\qquad P = \dfrac{\pi\bar{E}e_a E_y}{2E_a}$

The equation (2-38) can be changed to equation (2-39) by the use of Chebyshev polynomials.

$$\sum_{j=1}^{N} b_j \frac{\sin(j\frac{k\pi}{N})}{\sin(\frac{k\pi}{N})}\left[1 + \frac{\lambda}{j\pi}\sin\left(\frac{k\pi}{N}\right)\right] = -\frac{P}{\pi} \quad k = 1,2,\cdots N \tag{2-39}$$

The constant b_j can be obtained through the above equation and then $\varepsilon_x^{(2)}(\tau,\sigma)$ can be obtained.

(1) The equation (2-27) can be changed to the following equation from equations (2-17), (2-20) and (2-21).

$$\sum_{j=1}^{N} c_j \frac{\sin(j\frac{k\pi}{N})}{\sin(\frac{k\pi}{N})}\left[1+\frac{C_{31}a}{jAh}\sin\left(\frac{k\pi}{N}\right)\right]=0 \tag{2-40}$$

where $A=\frac{2G}{k+1}$, then τ_{xy} and ϕ can be obtained.

(2) σ can be obtained from the following equation which is changed from the equation (2-28).

$$\sigma=-C_{31}\cdot\phi \tag{2-41}$$

(3) In order to obtain σ_y and ψ, the equation (2-26) is changed to the following equation from equations (2-17), (2-20), (2-22), (2-31).

$$\sum_{j=1}^{N} d_j \frac{\sin(j\frac{k\pi}{N})}{\sin(\frac{k\pi}{N})}\left[1+\frac{C_{22}a}{jAh}\sin\left(\frac{k\pi}{N}\right)\right]=\frac{C_{21}}{A}\varepsilon_x-\frac{e_2E_y}{A} \tag{2-42}$$

(4) The following equation is the simple description of the equation (2-25) to obtain τ.

$$\tau=-(hC_{11}\varepsilon_x+C_{12}\psi) \tag{2-43}$$

Then from equation (2-5), the interfacial stress distributions of the piezoelectric actuator can be obtained.

3. Finite element analysis

The above analytical model was adopted to predict the stress distributions of the piezoelectric actuator in 3D situation. The ABAQUS software was used to numerically analyze the stress field of the 3D actuator model. The actuator material studied in this paper was Lead Zirconate Titanate-4 (PZT-4), and the material parameters are listed in Table 1 (Zhao *et al*. 2012). The host structure used in this paper was considered as an isotropic elastic material, E = 120GPa, $\upsilon=0.3$. The width of the actuator was fixed to 0.1 mm. In order to get a complete analysis, the length of the actuator had two sizes (2 mm and 6 mm) and the thickness of the actuator had also two sizes (2 mm and 4 mm). The various 3D actuator FEM models were used to get the validity of the 2D analytical model.

The 3D FEM model was shown in Fig. 3. The boundary conditions were all consistent. The bottom of the host structure was constrained. The other surfaces were free. And the only load was the electrical field which was uniformly applied to the upper and lower surface of the actuator. The 3D FEM mesh was shown in Fig. 4. The actuator was assigned as 8-node bilinear piezoelectric quadrilateral. In order to reduce the error, the denser mesh grids were applied along the ends of the actuator.

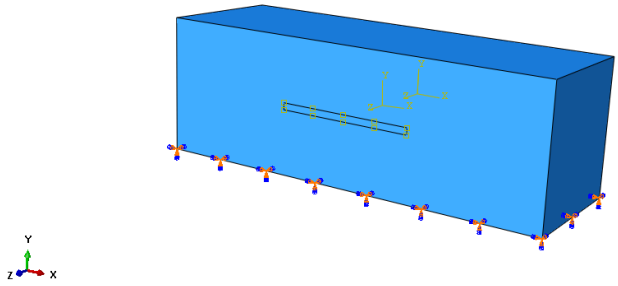

Fig. 3 The FEM model of the actuator modeling by the ABAQUS software

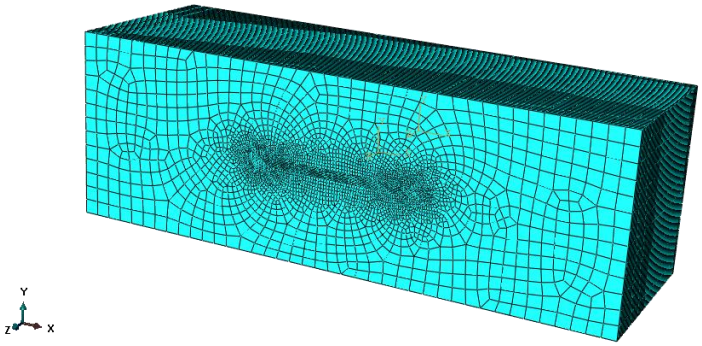

Fig. 4 The finite element model mesh

Table 1 Material properties of the piezoelectric actuator studied in this paper.

Elastic stiffness coefficients (GPa)					Piezoelectric coefficients (C/m^2)			Dielectric constants (10^{-9}C/Vm)	
C_{11}	C_{12}	C_{13}	C_{33}	C_{44}	e_{33}	e_{31}	e_{15}	λ_{11}	λ_{33}
139.0	67.8	74.3	115.0	25.6	15.1	-5.2	12.7	6.45	5.62

4. Results and discussion

In this paper, we denoteσ^+ and σ^- respectively as the interfacial normal stresses of the actuator's upper surface and lower surface obtained through the ABAQUS software. While σ_a^+ and σ_a^- are obtained through the formula derivation as the analytical results of the interfacial normal stresses. In the same, τ^+ and τ^- are obtained through the ABAQUS software as the FEM results of the interfacial shear stresses of the actuator's upper surface and lower surface. τ_a^+ and τ_a^- are obtained through the formula derivation as the analytical results of the interfacial shear stresses.

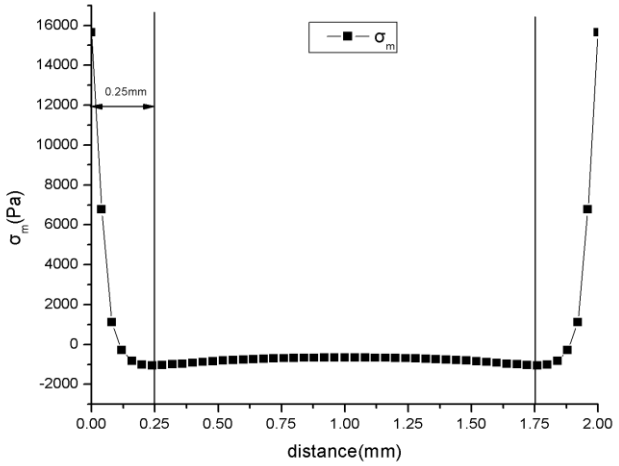

Fig. 5 Stress distribution of σ_m in the thickness direction (the horizontal axis denotes the distance of points away from the front surface and the vertical axis denotes the normal stress of the points)

We denote $\sigma_x$as the FEM result of the axial normal stress of the actuator's midsection. And σ_x^a are obtained through the formula derivation as the analytical result of the axial normal stress.

From the theory of Elastic Mechanics, we can get that the actuator can be treated as a plane stress state when its thickness is very small and the actuator can be treated as a plane strain state when its thickness is larger enough. When the actuator is in plane stress state, the stress of the actuator occurs only in the plane. When the actuator is in plane strain state, the strain of the actuator occurs only in the plane. Based on this we discuss the validity of the 2D analytical model to predict 3D actuator model.

The stress distributions of σ_y in thickness direction are obtained through the ABAQUS software. We choose the stress distribution of the middle section (noted as σ_m) to indicate the actuator's stress state, as shown in Fig. 5. From the figure, we can see that the stress of the points about 0.25 mm away from the front/rear surface has large change with the distance. We think that at this space the actuator is in plane stress state. While in the middle part, the stress has no obvious change. We think that at this space the actuator is in plane strain state. The numerical results are shown in the following part.

4.1 Interfacial stresses and axial normal stress in plane stress state (the thickness of the actuator is 2 mm)

4.1.1The length of the actuator is 2 mm

The above three figures (Fig. 6-Fig. 8) show the stress distributions of the piezoelectric actuator under electrical loadings in plane stress state. The FEM results are obtained from the stresses at the positions about 0.12 mm away from the front surface. Because the strain in z direction was not taken into account, a little difference existed between the analytical results and the FEM results,

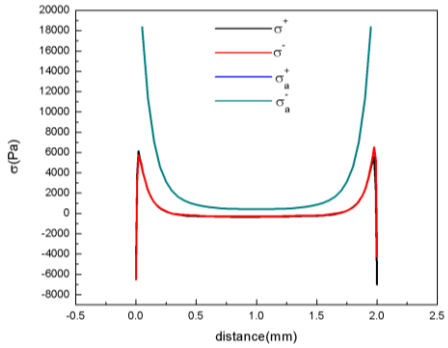

Fig. 6 Interfacial normal stresses of the 2 mm actuator in plane stress state (the horizontal axis denotes the distance of points in the section away from the end of the actuator and the vertical axis denotes the interfacial normal stress of the points)

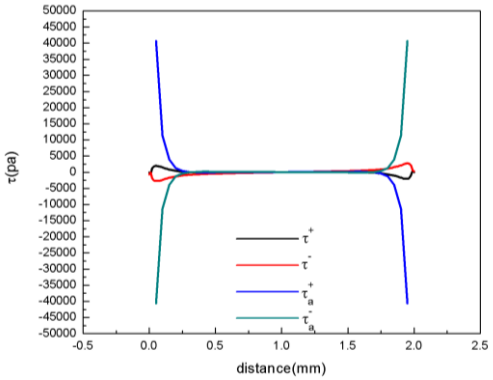

Fig. 7 Interfacial shear stresses of the 2 mm actuator in plane stress state (the horizontal axis denotes the distance of points in the section away from the end of the actuator and the vertical axis denotes the shear stress of the points)

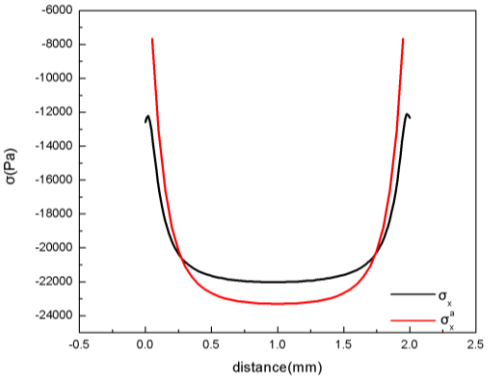

Fig. 8 Axial normal stresses of the 2 mm actuator in plane stress state (the horizontal axis denotes the distance of points in the section away from the end of the actuator and the vertical axis denotes the axial normal stress of the points

especially at the ends of the actuator. But when we ignore the stresses at both ends of the actuator, we can find that the two results are similar: the same tendency and a little difference in magnitude. For the 2 mm actuator, the stress distributions of the actuator between 0.5 mm to 1.5 mm can be predicted relative accurately.

4.1.2The length of the actuator is 6 mm

The PWM motor speed controller is expected to vary the 12V DC supply to the motor such that the speed of the motor becomes varied in steps. The realization circuit is shown in Fig. 2.

The heart of this system is the IC, CD4093 which is a quad 2 input NAND Schmitt trigger (Shinde *et al*. 2002). The system is operated from the 12V DC power supply at a current level of 5A. The Schmitt triggers from four in 4093, that is U1a cable with cycle oscillator is adjustable.

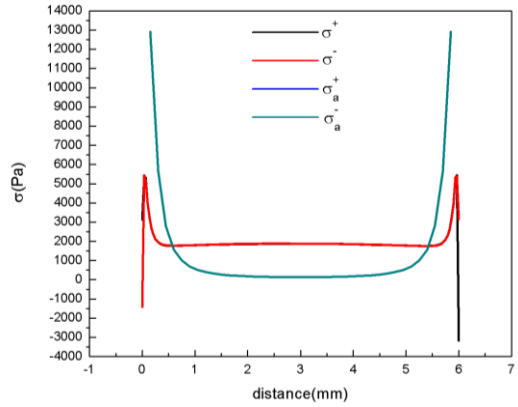

Fig. 9 Interfacial normal stresses of the 6 mm actuator in plane stress state (the horizontal axis denotes the distance of points in the section away from the end of the actuator and the vertical axis denotes the interfacial normal stress of the points)

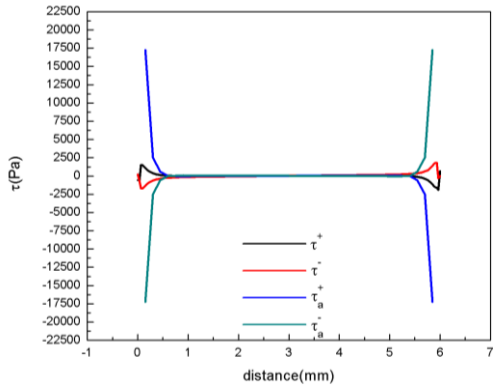

Fig. 10 Interfacial shear stresses of the 6 mm actuator in plane stress state (the horizontal axis denotes the distance of points in the section away from the end of the actuator and the vertical axis denotes the shear stress of the points)

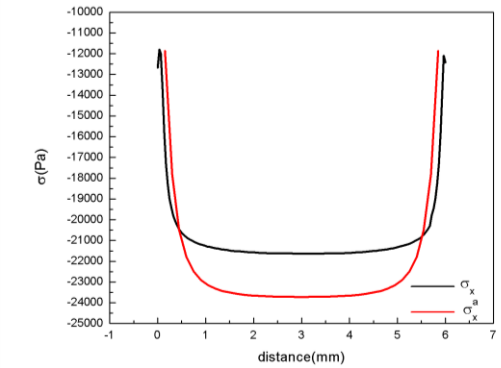

Fig. 11 Axial normal stresses of the 6 mm actuator in plane stress state (the horizontal axis denotes the distance of points in the section away from the end of the actuator and the vertical axis denotes the axial normal stress of the points)

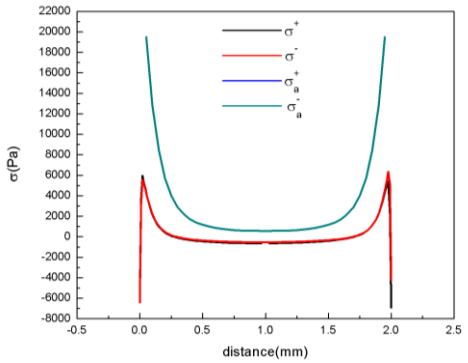

Fig. 12 Interfacial normal stresses of the 2 mm actuator in plane strain state (the horizontal axis denotes the distance of points in the section away from the end of the actuator and the vertical axis denotes the interfacial normal stress of the points)

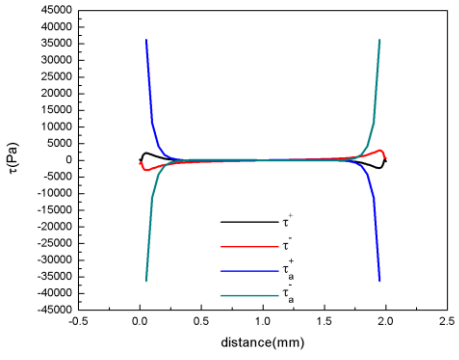

Fig. 13 Interfacial shear stresses of the 2 mm actuator in plane strain state (the horizontal axis denotes the distance of points in the section away from the end of the actuator and the vertical axis denotes the shear stress of the points)

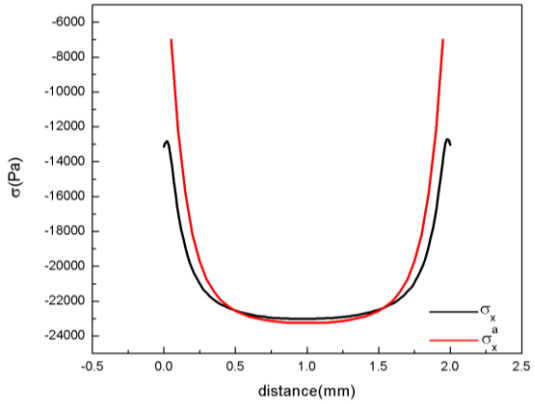

Fig. 14 Axial normal stresses of the 2 mm actuator in plane strain state (the horizontal axis denotes the distance of points in the section away from the end of the actuator and the vertical axis denotes the axial normal stress of the points

The U1b, U1c, U1d are buffer output from the oscillator to drive the switching MOSFET, Q1. The DC motor drives in accordance with the switching pulses from the oscillator. When R2 is varied, cycle varied and so is the motor speed (Ahmed and Alam 2013). Diodes D1 and D2 provides current paths between 4093 and R2, thus inhibiting current re-flux into the IC. Hence, 1N4004, a rectifier diode is chosen. R1 is a small value resistor which splits out current to R2, thus preventing overload current at low resistance. Hence, 1kΩ is chosen.

4.2 Interfacial stresses and axial normal stress in plane strain state (the thickness of the actuator is 2 mm)

4.2.1 The length of the actuator is 2 mm

The above three figures (Fig. 12-Fig. 14) show the stress distributions of the piezoelectric actuator under electrical loadings in plane strain state when the length of the actuator is 2 mm. The FEM results are obtained from the stresses at the positions of the middle section. Comparing with the plane stress state, we can find that the FEM results obtained in plane strain state show a better agreement with the analytical results, that is, the difference between the FEM results and the analytical results is reduced. For the 2 mm actuator, the stress distributions of the actuator between 0.5 mm to 1.5 mm can be predicted relative accurately.

4.2.2 The length of the actuator is 6 mm

When the length of the actuator is 6 mm, the stress distributions of the piezoelectric actuator are shown in Fig. 15 - Fig. 17. The FEM results are obtained from the stresses at the positions of the middle section. We can see that as the length of the actuator in plane strain state increases, the results have no obvious change such as the interfacial normal stresses and the interfacial shear stresses. Only the difference between the FEM results and the analytical results of the axial normal stresses is reduced as the length of the actuator increases. For the 6 mm actuator, the stress distributions of the actuator between 1 mm to 5 mm can be predicted relative accurately.

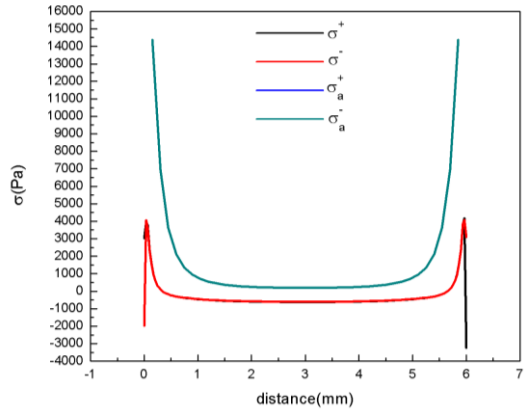

Fig. 15 Interfacial normal stresses of the 6 mm actuator in plane strain state (the horizontal axis denotes the distance of points in the section away from the end of the actuator and the vertical axis denotes the interfacial normal stress of the points)

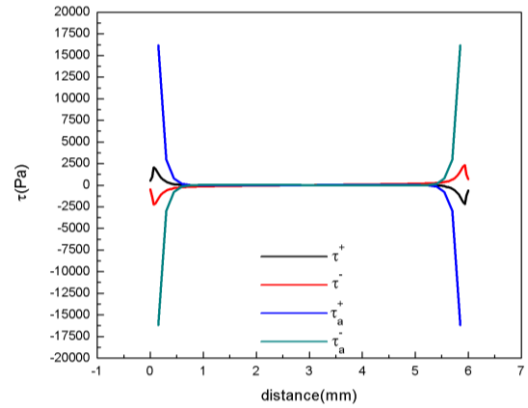

Fig. 16 Interfacial shear stresses of the 6 mm actuator in plane strain state (the horizontal axis denotes the distance of points in the section away from the end of the actuator and the vertical axis denotes the shear stress of the points)

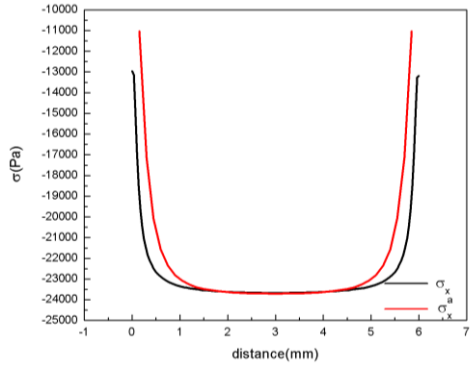

Fig. 17 Axial normal stresses of the 6 mm actuator in plane strain state (the horizontal axis denotes the distance of points in the section away from the end of the actuator and the vertical axis denotes the axial normal stress of the points)

4.3 Interfacial stresses and axial normal stress when the thickness of the actuator is 4 mm

4.3.1 The thickness of the actuator is 4 mm (in plane stress state)

The above three figures (Fig. 18-Fig. 20) show the stress distributions of the piezoelectric actuator under electrical loadings in plane stress state when the length of the actuator is 2 mm and the thickness of the actuator is 4 mm. The FEM results are obtained from the stresses at the positions about 0.24 mm away from the front surface. We can see that as the thickness of the actuator increases, the FEM results of the interfacial normal stresses and the axial normal stresses show a better agreement with the analytical results. The interfacial shear stresses have no obvious change as the thickness of the actuator increases. For the 2 mm actuator, the stress distributions of the actuator between 0.5 mm to 1.5 mm can be predicted relative accurately.

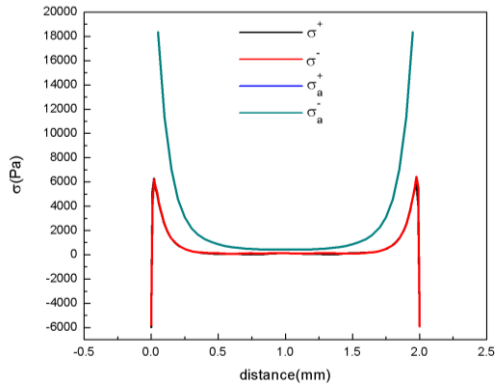

Fig. 18 Interfacial normal stresses when the thickness of the actuator is 4 mm in plane stress state (the horizontal axis denotes the distance of points in the section away from the end of the actuator and the vertical axis denotes the interfacial normal stress of the points)

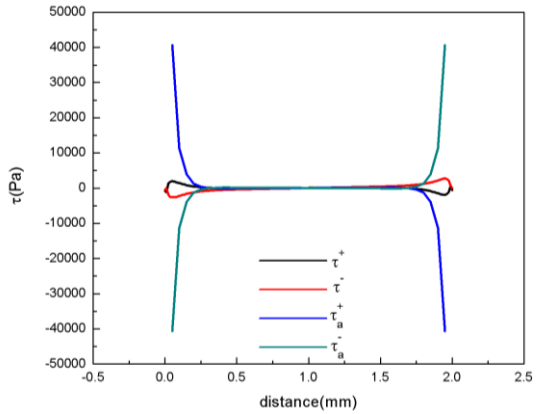

Fig. 19 Interfacial shear stresses when the thickness of the actuator is 4 mm in plane stress state (the horizontal axis denotes the distance of points in the section away from the end of the actuator and the vertical axis denotes the interfacial normal stress of the points)

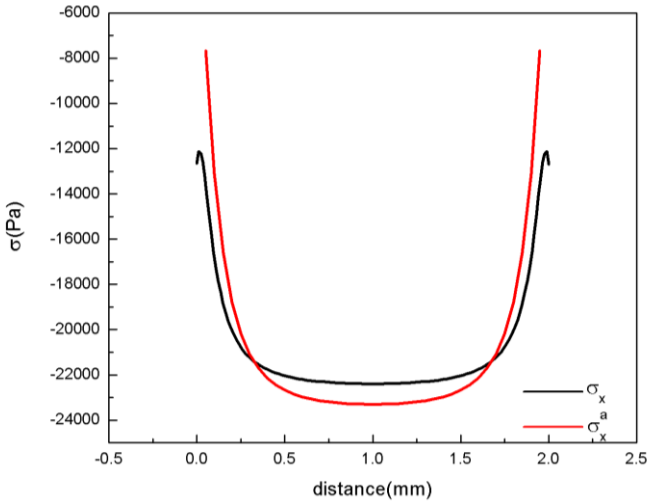

Fig. 20 Axial normal stresses when the thickness of the actuator is 4 mm in plane stress state (the horizontal axis denotes the distance of points in the section away from the end of the actuator and the vertical axis denotes the interfacial normal stress of the points)

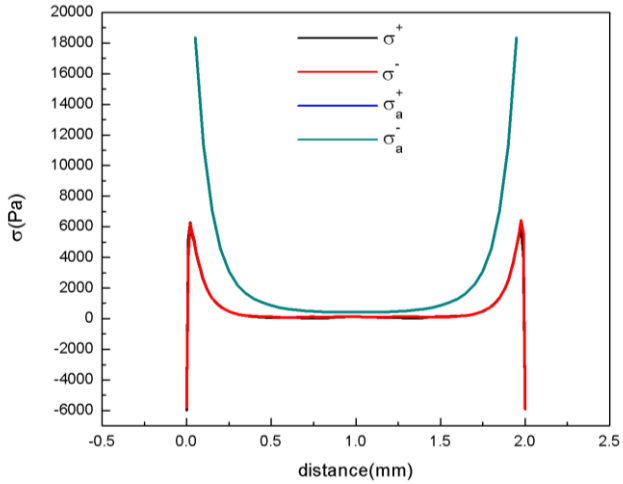

Fig. 21 Interfacial normal stresses when the thickness of the actuator is 4 mm in plane stress state (the horizontal axis denotes the distance of points in the section away from the end of the actuator and the vertical axis denotes the interfacial normal stress of the points)

4.3.2 The thickness of the actuator is 4 mm (in plane strain state)

When the actuator is in plane strain state, the stress distributions of the piezoelectric actuator under electrical loadings are shown in Fig. 21-Fig. 23. The FEM results are obtained from the stresses at the positions of the middle section. Comparing with the plane stress state, the difference between the FEM results and the analytical results of the interfacial stresses in plane strain state is increased, while the difference between the two results of the axial normal stresses is reduced. The interfacial shear stresses still have no obvious change. For the 2 mm actuator, the stress distributions of the actuator between 0.5 mm to 1.5 mm can be predicted relative accurately

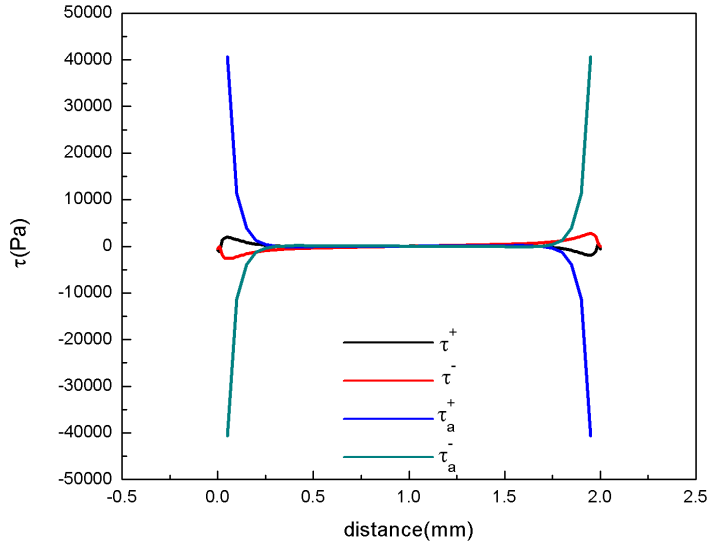

Fig. 22 Interfacial shear stresses when the thickness of the actuator is 4 mm in plane stress state (the horizontal axis denotes the distance of points in the section away from the end of the actuator and the vertical axis denotes the interfacial normal stress of the points)

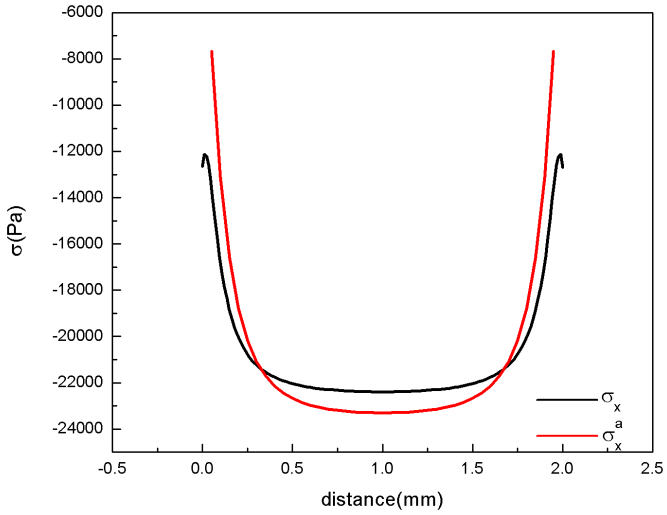

Fig. 23 Axial normal stresses when the thickness of the actuator is 4 mm in plane stress state (the horizontal axis denotes the distance of points in the section away from the end of the actuator and the vertical axis denotes the interfacial normal stress of the points)

5. Conclusions

In this paper, we adopted a two-dimension alanalytical electro-elastic model to predict the stress distributions of the PZT actuator in 3D situation. The interfacial stresses and the axial normal stress in both plane stress state and plane strain state were obtained to study the actuation

effects being transferred from the actuator to the host. We analysedthe stress distributions of the PZT actuator in different length and different thickness to guarantee the generality and the error intervals were given. The numerical results showed that it is feasible for adopting the 2D analytical to predict the stress distributions in 3D situation. We can also conclude that when the actuator is in plane strain state, the FEM results show a better agreement with the analytical results. As the thickness of the actuator increases, the difference between the FEM results and the analytical results is reduced.

The validity of the present model has been demonstrated by application to specific examples and comparison with the corresponding results obtained from the Finite Element Method. The results can serve as a design tool for estimation of optimum piezoelectric element thickness, i.e., from thin film to a beam like structure. As the deformation of z-axial direction was not taken into consideration in the paper, the model had some errors. And we would make further research on the model in the future.

Acknowledgment

The authors appreciate the financial supports from National Nature Science Fund of China (51210008, 50905142), Fundamental Research Fund(JC201138,JC2010230 and JC20120231) at Northwestern Polytechnical University and 111 project (B07050).

References

Crawley, E.F. and Lazarus, K.B. (1991), "Induced strain actuation of isotropic and anisotropic plates", *AIAA J*., **29**, 944-951.

Crawley, E.F. and De Luis, J. (1987), "Use of piezoelectric actuators as elements of intelligent structures", *AIAA J*., **25** (10), 1373-1385.

Crawley, E.F. and Anderson, E.H. (1990), "Detailed models of piezoceramic actuation of beams", *J. Intelligent. Mater. Syst. Struct*., **1**, 4-25.

Im, S. and Atluri, S.N. (1989), "Effects of a piezo-actuator on a finite deformation beam subjected to generalloading", *AIAA J*., **27**, 1801-1807.

Lin, M.W. and Rogers, C.A. (1993), "Actuation response of a beam structure with induced strain actuators", *Adaptive Struck. Mater. Syst*., **35**, 129-139.

Lee, C.K. Moon, F.C. (1989), "Laminated piezopolymer plates for torsion and bending sensors andactuators", *J. Acoust. Soc. Am*., **85**, 2432-2439.

Tzou, H.S. and Gadre, M. (1989), "Theoretical analysis of a multi-layered thin shell coupled with piezoelectricshell actuators for distributed vibration control", *J. Sound Vibrat*., **132**, 433-450.

Qiu, Z.C., Zhang, X.M., Wu, H.X. and Zhang, H.H. (2007), "Optimal placement and active vibration control for piezoelectric smart flexible cantilever plate", *J. Sound Vibrat*., **301**, 521-543.

Kumar, R., Mishra, B.K. and Jain, S.C. (2008), "Static and dynamic analysis of smart cylindrical shell", *Finite Elem. Anal. Des*., **45**, 13-24.

Wang, X.D. and Huang, G.L. (2006), "Wave propagation generated by piezoelectric actuators attached to elastic substrates", *Acta .Mech*,, **183**, 155-176.

Wang, B.T. and Rogers, C.A. (1991), "Laminated plate theory for spatially distributed induced strainactuators", *J. Compos.Mater*., **25**, 433-452.

Wang, X.D. and Meguid, S.A. (2000), "On the electro-elastic ehavior of a thin piezoelectric actuator attached to an infinite host structure", *Int. J. Solids Struct*. **37**, 3231-3251.

Wang. X.D. and Huang, G.L. (2001), "The electromechanical behavior of a piezoelectric actuator bounded to an anisotropic elastic medium", *Int. J. Solids Struct*., **38**, 4721-4740.

Zhao, B. and Wang, X.D. (2012), "Modelling of Electroelastric Behaviour of Embedded Piezoelectric Actuators in Smart structures: 2D and 3D effects", *Adv. Mater. Res*., **569**, 207-214.

Zheng, S.J., Dai, F. and Song, Z. (2009), "Active control of piezo the rmalelastic FGM shells using integrated piezoelectric sensor/actuator layers", *Int. J. Appl. Elect*.., **30**, 107-124.

Zhuk, Y.A. and Senchenkov, I.K. (2010), "Modeling the stationary vibration and dissipative heating of thin-walled inelastic elements with piezoactive layers", *Int. Appl. Mech*. 2004, **40**, 546-556.